


How molecular effects affect solutal Marangoni flows

Petter Johansson * and Guillaume Galliéro 

*Laboratoire des Fluides Complexes et Leurs Réservoirs,
Université de Pau et des Pays de l'Adour, E2S UPPA, CNRS, Total, LFCR, 64000 Pau, France*

Dominique Legendre 

*Institut de Mécanique des Fluides de Toulouse (IMFT),
Université de Toulouse, CNRS-INPT-UPS, 31400 Toulouse, France*



(Received 25 June 2021; accepted 1 June 2022; published 22 June 2022)

Interfacial tension gradients drive flow along fluid-fluid interfaces in a process known as the Marangoni effect. Such gradients can be caused by surfactants, as extensively studied in the literature. Less is known of its nanoscale behavior, where molecular interfaces exhibit specific properties such as interfacial viscosity. In this work we study the solutal Marangoni effect at a model fluid-fluid interface using molecular dynamics simulations. We show that molecular interfacial effects are important and should be accounted for in nanofluidic regimes. Hydrodynamic models can be extended with effective terms that include them.

DOI: [10.1103/PhysRevFluids.7.064202](https://doi.org/10.1103/PhysRevFluids.7.064202)

I. INTRODUCTION

The Marangoni effect (also called the Gibbs-Marangoni effect) describes liquid transport along fluid-fluid interfaces from regions of low-to-high surface or interfacial tension [1,2]. It is a powerful effect, requiring only small interfacial tension gradients to create strong convective flows. Such gradients arise naturally by the addition of a surfactant at a liquid interface, as has been studied in various configurations using both experiments [3] and continuum fluid dynamics simulations [4]. This solutal Marangoni effect plays a role in many phenomena, in particular foam and emulsion formation and evolution [5].

The phenomena is well understood from the macroscopic point of view, where the induced shear stress leads to flows proportional to the interfacial tension gradient [1]. However, less is known on possible microscopic effects on such phenomena when the width of the interface is not negligible compared to the size of the bubble or droplet, such as when considering nanoemulsion, nanobubbles, or nanodroplets [6–8]. In this paper we will show how molecular details influence the solutal Marangoni effect of a model fluid-fluid interface populated with surfactant molecules.

Molecular dynamics simulations have shown to be an efficient complementary tool to experiments to better understand flows at the nanoscale, in particular close to interfaces [9–11]. Regarding solutal Marangoni flow, molecular dynamics simulations have been used to confirm that nanoscopic interfacial tension gradients induce molecular flows [12,13] and that the right force leading to Marangoni flow is related to chemical potential gradients [14].

Less is known of how surfactants and molecular details affect the flow features at the nanoscale. At such scales interfaces themselves are of nonzero width and display properties separate from the bulk phases, especially in the presence of surfactants. For example, momentum is not transferred perfectly across fluid-fluid interfaces when a shear stress is applied tangential to the interface. This

*pjohansson@univ-pau.fr

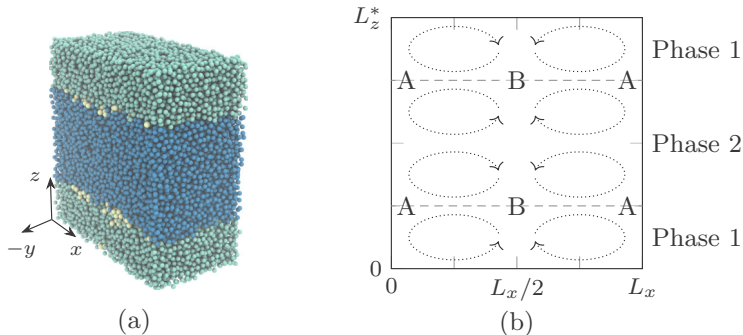


FIG. 1. (a) Simulated two-phase system with surfactants at interfaces (white). (b) Two-dimensional view with low (A) and high (B) surfactant concentration zones marked. Steady state flow vortices are sketched. Figures are created with VMD, MATPLOTLIB, and PGFPLOTS [23–25].

corresponds to a partial slip between the fluid phases [15–22], which alters the viscous dissipation across the phase boundary. The effect can be characterized by an interfacial viscosity

$$\mu_I = \frac{\tau_{xz}w}{\Delta u_{x,I}}, \quad (1)$$

where τ_{xz} is a tangential shear over the interface (which is normal to z), w the interface width, and $\Delta u_{x,I}$ the change in velocity over that width. While this contribution to the dissipation in a system is negligible on a macroscopic scale it is important to account for as we approach the nanoscale. Furthermore, as the Marangoni effect induces strong shear stresses at the interface, the effect will be important to understand for hydrodynamic modeling of nanoscale Marangoni systems.

With this work we use nonequilibrium molecular dynamics simulations to investigate the solutal Marangoni effect on a molecular scale. In particular the varying interfacial viscosity is shown to have a large influence as molecular length scales are approached. We show how this effect can be accounted for in hydrodynamic modeling by knowing how liquid properties vary with the local surfactant concentration, which becomes the only required interfacial parameter in addition to usual macroscopic qualities.

II. METHOD

To start we consider a two-phase system with liquid phases 1 and 2 shown in Fig. 1. The phases are immiscible and separated along the z axis by two interfaces. Both phases consist of dimer Lennard-Jones molecules with identical atoms of mass m . Intermolecular interactions between atoms in phase i and j are given by the Lennard-Jones potential

$$U_{ij}(r) = 4\varepsilon_{ij} \left(\frac{\sigma_{ij}^{12}}{r^{12}} - \frac{\sigma_{ij}^6}{r^6} \right), \quad (2)$$

where r is the distance between the atoms and ε_{ij} , σ_{ij} the interaction parameters. Phases 1 and 2 are made identical by setting $\varepsilon_{11} = \varepsilon_{22} \equiv \varepsilon$ and $\sigma_{11} = \sigma_{22} \equiv \sigma$ and immiscible by setting the cross-interaction strength $\varepsilon_{12} = 0.5\varepsilon$. Internal harmonic bonds with strength $k = 1000\varepsilon$ and distance σ keep the atoms of the dimers together. Surfactant molecules are created as identical dimers where one atom is of species 1 and the other of species 2: the first is attracted to phase 1, the other to phase 2. By doing so, the surfactant molecules place themselves naturally at the fluid-fluid interface.

Simulations are performed and results presented in Lennard-Jones reduced units [26] with $\varepsilon = \sigma = m = k_B = 1$, where k_B is the Boltzmann constant. The temperature is $T = 0.8$ and bulk atom number density in the liquid phases is $\rho_b = 0.87$. Without surfactants the interfacial tension

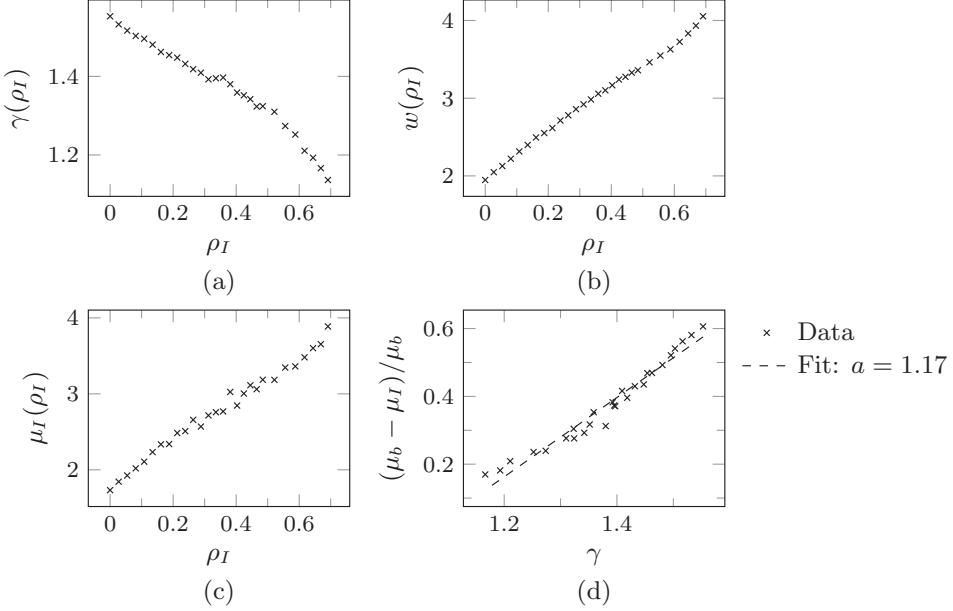


FIG. 2. (a) Interfacial tension γ , (b) width w , and (c) viscosity of the interface μ_I for various surfactant concentrations ρ_I at the fluid-fluid interface. (d) Both sides of (3) shown for our data with a linear fit.

of the two-phase interface is measured to be $\gamma_0 = 1.5$. Using nonequilibrium molecular dynamics [27–29] the shear viscosity of the bulk is measured to be $\mu_b = 4.4$. Simulations are performed with GROMACS 2020 [30,31] using a leapfrog integrator with a time step $dt = 0.002$ and interaction cutoff range $r_c = 3.5$. Periodic boundary conditions are enforced along all dimensions. Temperature is controlled with a velocity rescaling thermostat [32] with coupling time $t_c = 5.0$.

To characterize the influence of surfactant concentration ρ_I at the interface we measure how local properties vary with it at equilibrium. Our required properties are the interfacial tension $\gamma(\rho_I)$, interface width $w(\rho_I)$, and interfacial viscosity $\mu_I(\rho_I)$. Measurements are done using the following procedure: First, surfactant molecules are inserted in equal amounts at the two liquid-liquid interfaces and an equilibration simulation is run to achieve a consistent bulk density ρ_b . The box size is $L_x = L_y = 20$ along x and y and L_z along z . Each liquid phase has height 20. Second, an NVT simulation of 10^7 steps is run. From this simulation, the surfactant concentration (atom number density) ρ_I is defined by matching a Gaussian distribution $\rho(z) = \rho_I \exp[-a(z - z_i)^2]$ to each interface at position z_i and taking the mean. The interfacial tension $\gamma(\rho_I)$ is simultaneously calculated from the pressure tensor fluctuations inside the box [26]. Finally, following Ref. [17] a shear τ_{xz} is created in the system using the same method as when measuring μ_b . The shear simulation is run for 2×10^6 steps to create a steady state, after which data is collected over 2×10^7 steps. We then calculate the interfacial width $w(\rho_I)$ as the distance between where the density profiles of phase 1 and 2 reach $\rho = 0.95\rho_b$, which allows us to measure $\Delta u_{x,I}(\rho_I)$ and calculate $\mu_I(\rho_I)$ using (1) (see Figs. S1 and S2 in the Supplemental Material [33]). Measurements are repeated for a range of $\rho_I \in [0, 0.7]$ (see Fig. 2).

To perform the nonequilibrium simulations, those dedicated to studying Marangoni flows, an exchange scheme is deployed to create the zones of low and high ρ_I seen in Fig. 1(b). For each interface we define an edge zone A centered at $x = 0$ and a center zone B at $x = L_x/2$. Each zone is of size 2×2 along x and z and spans the entire width in y . At every N step of the simulation we check whether a surfactant molecule exists in zone A and if so exchange its type (Lennard-Jones interaction parameters) with a liquid molecule in zone B and vice versa. This scheme mimics that

of Liu *et al.* [14] except focused at the interfaces and applied to dimers instead of monomers. The position and momentum of the molecule remaining in each zone is not changed, only the molecule type. Since all molecules are of equal size and mass we preserve local momentum. If the exchange frequency N is sufficiently high a gradient $d\rho_I/dx$ forms along the interface.

Since the interfacial tension decreases with increasing surfactant concentration, a Marangoni flow develops between the zones to equilibrate the chemical potential. By maintaining the imbalance a steady state flow develops. Simulation systems are prepared and equilibrated following these steps for varying sizes $L_x = L_z \in [10, 100]$, with the size along y kept at a constant $L_y = 20$. The final box size along z after the surfactants have been added and system equilibrated is $L_z^* > L_z$. The exchange step frequency is $N = 500$. For each system size we start four independent nonequilibrium simulations, each of which runs for between 5×10^7 and 5×10^8 steps. We discard data from the first 2×10^6 steps to allow for the flow field in the system to develop. This is verified by comparing to data from the second half of the simulation. Finally, we collect the average flow field (mass and velocity) from the simulation in bins of size 0.25×0.25 along x and z .

III. RESULTS

Measurements of interfacial properties $\gamma(\rho_I)$, $w(\rho_I)$, and $\mu_I(\rho_I)$ are presented in Figs. 2(a)–2(c). As expected we see that the addition of molecular surfactants decreases the interfacial tension but increases the interface width and viscosity. These changes are mostly linear in the range of $\rho_I \in [0, 0.5]$, which as we will see contains the variation for all of our nonequilibrium simulations, but for higher concentrations we see a distinct nonlinear behavior as the surfactants start to form a separate phase of its own.

From a physical perspective it is clear how the presence of molecular surfactants link these quantities, but one may question if a relationship between them is in fact universal. A previous study [17] suggested that the interfacial viscosity can be deduced from the interfacial tension and bulk viscosity as

$$\frac{\mu_b - \mu_I}{\mu_b} = a\gamma \quad (3)$$

for some coefficient a that depends on the involved phases. We note that our data agrees well with this relationship for $a = 1.17$ [see Fig. 2(d)].

Turning to our nonequilibrium simulations, we present steady state surfactant density maps and flow streamlines for two systems in Fig. 3. We see that the steady state corresponds to a continuous gradient of surfactant concentration $\rho_I(x)$ along the interfaces and that a Marangoni driven flow develops in response to it. Looking at the flow fields in more detail we see that the flow vortices are not centered in each cell center. They trend towards a point that is two-thirds along the interface with a finite shift towards the center that is noticeable only for the smallest systems. We choose this vortex center point as the reference axis along z for comparing field data, since the flow will be most similar along it for all systems.

By measuring $\rho_I(x)$ along the interfaces we calculate our interfacial properties $\gamma(\rho_I) = \gamma(x)$ and $\mu_I(\rho_I) = \mu_I(x)$ along them through measurements in Fig. 2. We also measure the interfacial velocity $u_{x,I}(x)$ along the interfaces. These measurements are shown in Fig. 4 for $L_x = 40$. Results from more system sizes and a view of the described reference axis are available in Figs. S3–S6 of the Supplemental Material [33].

IV. DISCUSSION

Although the flow profiles look qualitatively consistent with what could be expected from a Marangoni driven flow (Fig. 3) a question arises: Can our simulated nanoscopic Marangoni flow be quantitatively described by continuum hydrodynamic modeling using the incompressible Navier-Stokes equation? Not if we neglect to model the interfaces molecular properties, as we will

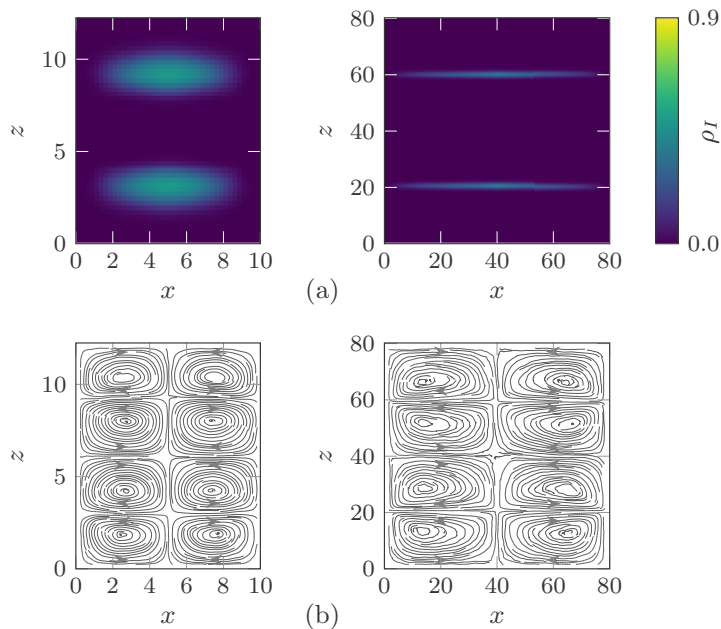


FIG. 3. (a) Surfactant density ρ_I and (b) velocity streamlines for steady state flow in systems of input size 10×10 and 80×80 .

now show. Marangoni convection velocity is related to the interfacial tension gradient $\nabla\gamma$ and the viscosity μ :

$$u_{x,I} \propto \frac{\nabla\gamma}{\mu_b}, \quad (4)$$

if we take the bulk shear viscosity μ_b . But in Figs. 4(b), 4(d) we see a velocity gradient at the center, where the interfacial tension gradient is constant. The effect remains even as we double the system size along x only (see Fig. S6 of the Supplemental Material [33]), thus this is not due to the finite size of the system or to hydrodynamic effects.

To model this velocity change we have to account for the interface itself. So what happens inside of it? In Fig. 5(a) we extract the velocity profile $u_x(z)$ through the reference axis of a 40×40 size system and denote the bulk and interface with different markers. We see that $u_x(z)$ is quadratic in each bulk phase, with a minima at the center and maximum at the interface, in agreement with a calculation of the expected flow as shown in Eq. (S27) of the Supplemental Material [33]. This is apparent by adjusting the minima to 0 and taking the square root, which results in a linear profile through the center bulk [Fig. 5(b)]. However, at the interface the linear slope changes, which indicates a change in viscosity inside the interface. This confirms the influence of the interfacial viscosity μ_I , defined by Eq. (1), on the local amplitude of the flow at the interface. See Figs. S7 and S8 in the Supplemental Material [33] for profiles of more system sizes.

We now consider how to describe the nanoscopic flow using hydrodynamics. In the Supplemental Material [33] we calculate the expected interface velocity $u_{x,I}$ using the continuum Navier-Stokes equation [Eq. (S27)]:

$$u_{x,I}(x) = \frac{\alpha H}{\mu} \frac{d\gamma}{dx}, \quad (5)$$

where H is the height of the flow-reverse-flow vortex along z , μ is the shear viscosity and α a prefactor, which is $\alpha = 1/6$ for the considered flow geometry, similar to those we observe at the

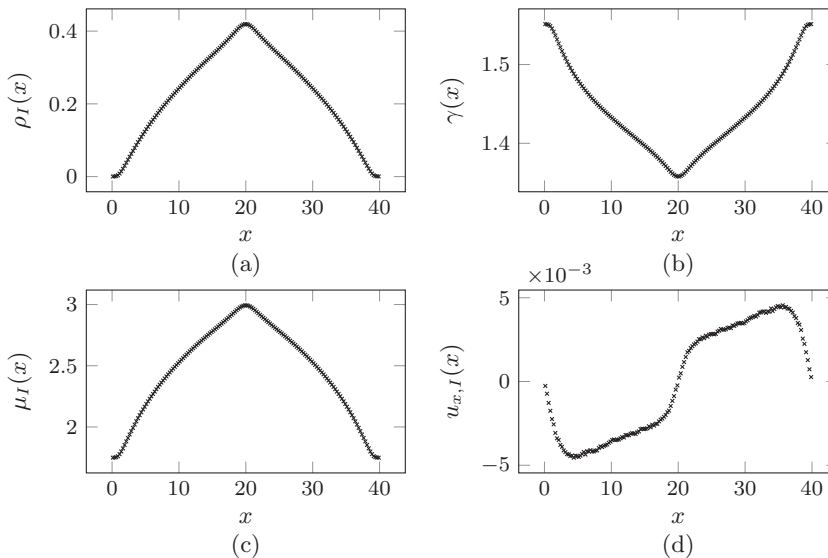


FIG. 4. (a) Measured surfactant concentration ρ_I , (b) interfacial tension γ , and (c) interfacial flow u_x along the phase boundaries for a system of size 40×40 .

vortex center axis in all our systems. If this model correctly describes the shear dissipation of our simulated systems, Eq. (5) should yield a constant α for our measured $u_{x,I}$, $d\gamma/dx$, and μ at these points.

With this in mind we measure α from our simulations in two ways for our full range of system sizes (see Fig. 6): First, using only the bulk phase dissipation, by setting $\mu = \mu_b$ and $H = L_z/4$ since there are four vortices along z . Here α changes dramatically for systems with $L_z < 40$, where the interface is prominent. For larger systems α is still higher than $1/6$.

Second, we include the interfacial dissipation by calculating the effective viscosity $\mu^*(x)$ using a harmonic average, as the shear is parallel to the interface [17]

$$\frac{w(x) + L_b(x)}{\mu^*(x)} = \frac{w(x)}{\mu_I(x)} + \frac{L_b(x)}{\mu_b}, \quad (6)$$

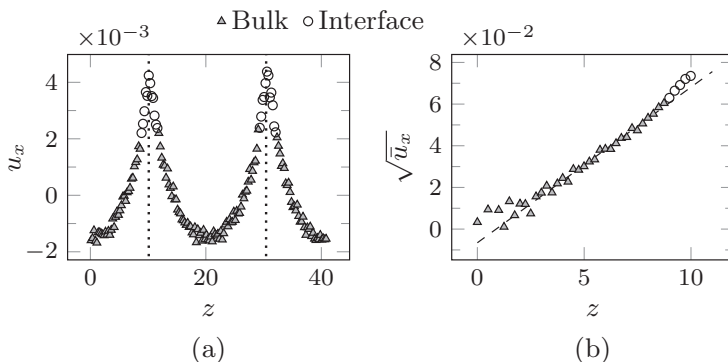
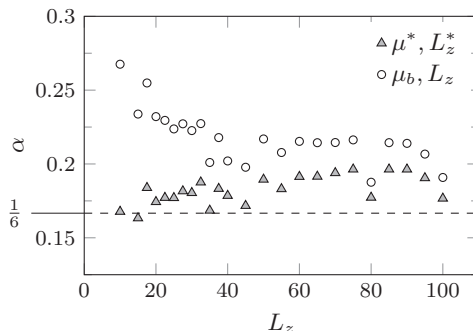


FIG. 5. (a) Velocity profile $u_x(z)$ for system size 40×40 . Interface centers are marked. (b) Square-root plot where $\bar{u}_x = u_x(z) - u_0$ adjusts the profile to its approximate minima. Linear fit of center bulk values drawn as a dashed line.


 FIG. 6. α coefficients for a range of system sizes $L_x = L_z$.

where $L_b(x) = L_z^*/2 - w(x)$ is the width of the bulk phases. Setting $H = L_z^*/4$ and $\mu = \mu^*$ to estimate α for our systems we obtain an improved agreement with the description. α is now constant and close to $1/6$. This last result, even if qualitative, confirms that such nanoscopic Marangoni flow can be well modeled by a continuum hydrodynamics approach if the local interfacial properties are taken into account.

V. CONCLUSIONS

From the results presented in this work on the modeling of a nanoscopic solutal Marangoni flow we make two conclusions: First, local finite interface features must be accounted for to model nanoscopic systems. This is shown by the inability to model the velocity gradient $u_{x,l}$ without accounting for the varying interface properties, here being interfacial tension, interface width, and interfacial viscosity. Second, this interfacial viscosity μ_l , which is included in the effective viscosity μ^* is a quantitative measure of the dissipation inside an interface and can be measured locally. While this work has focused on solutal Marangoni convection, this has implications for any systems, which model nanoscale flows with interfaces.

A few complications are of note. The assumptions made to derive Eq. (5) are simplified. In particular, our streamlines are not perfectly parallel to the interface along the vortex axis, but slightly tilted [Fig. 3(b)]. This leads to estimated coefficients, which are slightly higher than $\alpha = 1/6$. The tilt decreases for our smaller systems, where the measured α coefficients are closer to $1/6$. This supports the description as being qualitatively correct. Furthermore, our molecular modeling based on Lennard-Jones dimers is very simple. Further study into interfacial properties using more realistic liquid models are required to understand their real implications for nanoscale flows of practical interest.

ACKNOWLEDGMENTS

P.J. gratefully acknowledges Institut Carnot ISIFoR for the support of a postdoctoral grant. We also thank UPPA for providing computational facilities at the Pyrene cluster.

-
- [1] L. E. Scriven and C. V. Sternling, The Marangoni effects, *Nature (London)* **187**, 186 (1960).
 - [2] P.-G. de Gennes, F. Brochard-Wyart, and D. Qu  r  , *Capillarity and Wetting Phenomena* (Springer, New York, 2004)
 - [3] P. Bazazi and S. H. Hejazi, Retarding spreading of surfactant drops on solid surfaces: Interplay between the Marangoni effect and capillary flows, *Phys. Rev. Fluids* **5**, 084006 (2020).

- [4] O. Atasi, B. Haut, A. Pedrono, B. Scheid, and D. Legendre, Influence of soluble surfactants and deformation on the dynamics of centered bubbles in cylindrical microchannels, *Langmuir* **34**, 10048 (2018).
- [5] P. Walstra, Principles of emulsion formation, *Chem. Eng. Sci.* **48**, 333 (1993).
- [6] M. Firouzi and A. V. Nguyen, The Gibbs-Marangoni stress and nonDLVO forces are equally important for modeling bubble coalescence in salt solutions, *Colloids Surf. A* **515**, 62 (2017).
- [7] P. J. P. Espitia, C. A. Fuenmayor, and C. G. Otoni, Nanoemulsions: Synthesis, characterization, and application in bio-based active food packaging, *Comp. Rev. Food Sci. Safety* **18**, 264 (2019).
- [8] M. A. Hack, W. Kwiciński, O. Ramírez-Soto, T. Segers, S. Karpitschka, E. S. Kooij, and J. H. Snoeijer, Wetting of two-component drops: Marangoni contraction versus autophobing, *Langmuir* **37**, 3605 (2021).
- [9] J. C. Eijkel and A. van den Berg, Nanofluidics: What is it and what can we expect from it? *Microfluid. Nanofluid.* **1**, 249 (2005).
- [10] L. Bocquet and E. Charlaix, Nanofluidics, from bulk to interfaces, *Chem. Soc. Rev.* **39**, 1073 (2010).
- [11] N. Kavokine, R. R. Netz, and L. Bocquet, Fluids at the nanoscale: From continuum to subcontinuum transport, *Annu. Rev. Fluid Mech.* **53**, 377 (2021).
- [12] Y. Imai, T. Yamamoto, Y. Okano, R. Sato, and Y. Shigeta, Molecular dynamics simulation of the nanoscale solutal Marangoni convection, *ASEAN J. Chem. Eng.* **17**, 29 (2017).
- [13] Y. Imai, T. Yamamoto, A. Sekimoto, Y. Okano, R. Sato, and Y. Shigeta, Numerical investigation of the nano-scale solutal Marangoni convections, *J. Taiwan Inst. Chem. Eng.* **98**, 20 (2019).
- [14] Y. Liu, R. Ganti, H. G. A. Burton, X. Zhang, W. Wang, and D. Frenkel, Microscopic Marangoni Flows Cannot Be Predicted on the Basis of Pressure Gradients, *Phys. Rev. Lett.* **119**, 224502 (2017).
- [15] J. Koplik and J. R. Banavar, Slip, Immiscibility, and Boundary Conditions at the Liquid-Liquid Interface, *Phys. Rev. Lett.* **96**, 044505 (2006).
- [16] Y. Hu, X. Zhang, and W. Wang, Boundary conditions at the liquid–liquid interface in the presence of surfactants, *Langmuir* **26**, 10693 (2010).
- [17] G. Galliéro, Lennard-Jones fluid-fluid interfaces under shear, *Phys. Rev. E* **81**, 056306 (2010).
- [18] M. Bugel, G. Galliéro, and J. P. Caltagirone, Hybrid atomistic–continuum simulations of fluid flows involving interfaces, *Microfluid. Nanofluid.* **10**, 637 (2011).
- [19] S. Razavi, J. Koplik, and I. Kretschmar, Molecular dynamics simulations: Insight into molecular phenomena at interfaces, *Langmuir* **30**, 11272 (2014).
- [20] P. Poesio, A. Damone, and O. K. Matar, Slip at liquid-liquid interfaces, *Phys. Rev. Fluids* **2**, 044004 (2017).
- [21] S. Zhan, Y. Su, Z. Jin, M. Zhang, W. Wang, Y. Hao, and L. Li, Study of liquid-liquid two-phase flow in hydrophilic nanochannels by molecular simulations and theoretical modeling, *Chem. Eng. J.* **395**, 125053 (2020).
- [22] S. Ham, A. K. Narayanan Nair, S. Sun, and R. Qiao, Modulation of slippage at brine–oil interfaces by surfactants: The effects of surfactant density and tail length, *Phys. Fluids* **34**, 022106 (2022).
- [23] W. Humphrey, A. Dalke, and K. Schulten, VMD: Visual molecular dynamics, *J. Mol. Graphics* **14**, 33 (1996).
- [24] J. D. Hunter, Matplotlib: A 2d graphics environment, *Comput. Sci. Eng.* **9**, 90 (2007).
- [25] C. Feuersänger, PGFPlots—A LaTeX Package to create normal/logarithmic plots in two and three dimensions, 2020.
- [26] M. Allen and D. Tildesley, *Computer Simulation of Liquids* (Oxford University Press, Oxford, 2017).
- [27] P. Bordat and F. Müller-Plathe, The shear viscosity of molecular fluids: A calculation by reverse nonequilibrium molecular dynamics, *J. Chem. Phys.* **116**, 3362 (2002).
- [28] G. Galliéro, C. Boned, and A. Baylaucq, Molecular dynamics study of the Lennard-Jones fluid viscosity: Application to real fluids, *Ind. Eng. Chem. Res.* **44**, 6963 (2005).
- [29] G. Galliéro and C. Boned, Shear viscosity of the Lennard-Jones chain fluid in its gaseous, supercritical, and liquid states, *Phys. Rev. E* **79**, 021201 (2009).
- [30] M. J. Abraham, T. Murtola, R. Schulz, S. Páll, J. C. Smith, B. Hess, and E. Lindahl, GROMACS: High performance molecular simulations through multi-level parallelism from laptops to supercomputers, *SoftwareX* **1–2**, 19 (2015).

- [31] S. Páll, A. Zhmurov, P. Bauer, M. J. Abraham, M. Lundborg, A. Gray, B. Hess, and E. Lindahl, Heterogeneous parallelization and acceleration of molecular dynamics simulations in GROMACS, *J. Chem. Phys.* **153**, 134110 (2020).
- [32] G. Bussi, D. Donadio, and M. Parrinello, Canonical sampling through velocity rescaling, *J. Chem. Phys.* **126**, 014101 (2007).
- [33] See Supplemental Material at <http://link.aps.org/supplemental/10.1103/PhysRevFluids.7.064202> for additional figures and a derivation of (5).